Clim. Past Discuss., 8, 3251–3276, 2012
www.clim-past-discuss.net/8/3251/2012/
doi:10.5194/cpd-8-3251-2012

Climate of the Past Discussions

The East Asian summer monsoon at mid-Holocene: results from PMIP3 simulations

W. Zheng[1], B. Wu[1], J. He[1,2], and Y. Yu[1]

[1]LASG, Institute of Atmospheric Physics, Chinese Academy of Sciences, 100029, Beijing, China
[2]Graduate University of Chinese Academy of Sciences, 100049, Beijing, China

Received: 31 July 2012 – Accepted: 1 August 2012 – Published: 8 August 2012

Correspondence to: W. Zheng (zhengwp@mail.iap.ac.cn)

Published by Copernicus Publications on behalf of the European Geosciences Union.

Abstract

Ten Coupled General Circulation Models (CGCMs) participating the third phase of Paleoclimate Modeling Intercomparison project (PMIP3) are assessed for the simulations of East Asian Summer Monsoon (EASM) at both the present climate and mid-Holocene. Results show that the PMIP3 model median well captures the characteristics of the EASM, including the two distinct features of the Meiyu Front and the stepwise meridional displacement of the monsoon rainbelt. At mid-Holocene, the enhanced EASM is simulated by the PMIP3 models. The model median shows that the changes of surface air temperature and precipitation are within the range as indicated by the proxy data over the eastern China. Both the changes of monsoonal circulation and the water vapor content favor the increasing of summer precipitation. Regional features can be identified between models because of their different simulations of the above changes. The model spread for the surface air temperature (TAS) is relatively smaller when compared with that of PMIP2 models in both the Northern Hemisphere and the eastern China. However, the model spread of summer precipitation is larger among PMIP3 models, particularly in the lower reaches of Yangzi River. The TAS over Tibetan Plateau has a positive relationship with the precipitation in the lower reaches of Yangzi River, yet this relationship does not apply for those PMIP3 models in which the monsoonal precipitation is more sensitive to the changes of large-scale circulation.

1 Introduction

The mid-Holocene (MH, approximately 6000 yr before present (BP)) is one of the widely studied periods in the Quaternary, which was characterized by a warmer period than present that is also known as Holocene Megathermal. The most important forcing for the MH is the seasonal contrast of incoming solar radiation at the top of atmosphere (Berger, 1978) that leads to a different climate conditions rather than present climate. Therefore, it provides an opportunity to assess the ability of the Coupled General

CPD
8, 3251–3276, 2012

Circulation Model (CGCM), to understand the mechanisms in the coupled model and to contribute to the projection of the climate change in the future.

The mid-Holocene has been a major period of foci in both the first and second phases of the Paleoclimate Modeling Intercomparison project (PMIP). Fruitful results have been achieved that the changes of insolation strengthened the summer monsoon systems in the northern Hemisphere and the ocean plays an important role in regulating the large-scale features of atmospheric circulations (Joussaume et al., 1999; Braconnot et al., 2000; Zhao et al., 2005; Braconnot et al., 2007a, b; Zheng and Braconnot, 2012). The numerical simulations show broad agreements with the reconstructions of proxy data that indicating an enhanced hydrological cycle and large-scale atmospheric circulation (Bartlein et al., 2011) and expansion of boreal forest at mid- and high latitudes of the Northern Hemisphere (Prentice et al., 2000). However, large spread of model simulations in responses to the mid-Holocene forcings exists among models.

The East Asian area is featured by a monsoon climate. Due to the different thermal capacity of the continent and the ocean, warm low-pressure systems dominate over the continent during boreal summer and the subtropical high locates over the North Pacific. The thermal contrast leads to a prevailing southerly winds in summer and northerly winds in winter (Tao and Chen, 1987). Numerous studies have well documented the characteristics of the East Asian Summer Monsoon (Ding and Chan, 2005), however, it is still difficult for the CGCMs to realistically reproduce the distribution and magnitude of the summer precipitation in the East Asian monsoon area (Zhao et al., 1995; Jiang et al., 2005). The contributing factors to the EASM are more complex than that of the tropical monsoon systems, in which the Pacific and Indian Ocean SSTs and the snow cover in the Eurasia and the Tibetan Plateau are believed to be primary contributing factors to the activity of the East Asian summer monsoon (Ding and Chan, 2005). The EASM experienced a series of changes through the Holocene that provides an opportunity for the understanding of mechanism and feedbacks of the EASM. Studies of proxy data revealed that the Holocene megathermal reached a maximum during 7200–6000 yr BP in China. The surface air temperature is about 1–4 °C higher than present climate and

CPD
8, 3251–3276, 2012

the enhanced EASM prevailed over the eastern China with an increased precipitation about 40–100 % when compared with present observations (Yao et al., 1991; Shi et al., 1993). Evaluation shows that the PMIP2 models reproduced warmer and wetter summer climate conditions in East Asia during MH, in which the surface air temperature (TAS) increased by 0.89 °C and the precipitation was 5.8 % higher (Wang et al., 2010). However, regional biases compared with the reconstruction and large spreads between models are found, in particular over and around the Qinghai-Tibetan Plateau.

Inspired by previous studies, the objective of this study is firstly to document basic features of the EASM from the PMIP3 models pre-Industrial (PI) simulations and compared with the present climate observations. And then changes of EASM during MH and the model spread in the eastern China are discussed for a better understanding of the mechanisms of monsoon changes at MH and the inter-model differences. The manuscript is organized as follows: Sect. 2 describes the models and experiment protocols of MH; Sect. 3 shows the results of PMIP3 model simulations for the PI and MH experiments and compares with the observations and the proxy reconstruction; Sect. 4 discusses the inter-model differences in monsoon precipitation change over the eastern China and the main findings are concluded in Sect. 5.

2 Models and experiments

Within the framework of PMIP3, the mid-Holocene experiment is set up to examine the coupled model sensitivity to the change of insolation. The insolation pattern is standardized following Berger (1978), with an eccentricity of 0.018682, an obliquity of 24.105° and a precession of 0.87°. The greenhouse gases concentrations are set to the same as that in the pre-Industrial (PI) experiment, except that the CH_4 concentration reduces from 760 ppb to 650 ppb. Other boundary conditions, such as the aerosols, solar constant, vegetation, ice sheets, topography and coastlines are prescribed as the same as in the PI experiments.

CPD
8, 3251–3276, 2012

Ten coupled GCMs from the PMIP3 database are used in this study (Table 1). The climatology is derived from the 100 yr output for each model. Because the number of simulations is small and the model simulations are not symmetrically distributed around the ensemble mean, the model median are considered when evaluating the PMIP3 models simulations. With this solution, outliers have less weight in the analysis. Since the PMIP3 models have different resolutions, a bilinear interpolation was firstly applied to interpolate different climate variables onto the common $1^{\circ} \times 1^{\circ}$ grid. At each grid point and for each variable, the values of model simulations were then sorted from minimum to maximum in order to extract the median value. Since a different model may be chosen as the median at each grid point, there is no inherent direct physical linkage between different fields; they only provide orders of magnitude and the large-scale patterns showing how well the PMIP3 ensemble captures the climatology over East Asia. In addition, the climatology from the CPC Merged Analysis of Precipitation (CMAP, Xie and Arkin, 1997) and the Climatic Research Unit (CRU, Mitchell and Jones, 2005) data are used for the evaluation of precipitation and land near-surface temperature, respectively. The National Center for Environmental Prediction (NCEP, Kalnay et al., 1996) data are used for the comparison of the monsoon circulations.

3 PMIP3 model results

3.1 Present climate

Figure 1a and c show the precipitation and TAS of present observation during the boreal summer (June, July and August averaged), respectively. Overall, the PMIP3 model median simulates the similar large-scale patterns of the monsoonal precipitation and TAS. The gradually decreasing of monsoonal rainfall from the tropics towards high latitude and the northwest part of China are captured (not shown). For the EASM, another dominant feature of the rainbelt extending from the middle and lower reaches of the Yangzi River to the east of Japan, also known as Meiyu in China and Baiu in Japan,

CPD
8, 3251–3276, 2012

is also reproduced by the model median but with a weaker precipitation. The large-scale monsoonal circulation over East Asia in PMIP3 model median broadly resembles that in the NCEP reanalysis (Fig. 2a). The southwesterly from the Indian Ocean brings water vapor to the East Asia while the vertical velocity at 500 hpa controls the pattern of monsoonal precipitation. The western Pacific is controlled by the subtropical high and its ridge plays an important role in determining the position of rainbelt.

However, several differences can be identified between the model median and the observed. The magnitude of precipitation is significantly underestimated by PMIP3 model median, particularly in the Bay of Bengal, the eastern China and the western Pacific (Fig. 1b). The TAS is cooler in the model median over most part of the East Asia when compared with the CRU data (Fig. 1d). It is also cooler over the ocean that may influence the monsoonal circulations. Although the green house gases are lower in the PI simulations than present climate, which could explain about 0.6 °C cooling biases between model and observations (Folland et al., 2001), the PMIP3 model median still has a cold bias over most area of East Asia (Fig. 1d). Larger coolings are found over the continent where excess monsoonal precipitation is simulated, for example over the Plateau Tibetan and Northern China (Fig. 1b). The differences in monsoonal circulation (Fig. 2b) explain the bias of precipitation in the model median, anomalous anticyclone and weaker updraft at 500 hpa locate in the Bay of Bengal and the southeast China that leads to weaker monsoonal rainfall, while the enhanced updraft corresponds to a stronger precipitation in the model median. In the northwest Pacific, the simulated precipitation is much weaker than the observation that is related with the cooler sea surface temperature (SST) simulated in the warm pool region and the tropics.

The seasonal cycle of monsoonal rainfall over Eastern China (averaged from 100° E to 120° E) is presented in Fig. 3, which indicates the seasonal march and retreat of the EASM. The stepwise meridional displacement is one of the most distinctive features of EASM compared with other tropical monsoon systems (Tao and Chen, 1987). The PMIP3 model median broadly reproduces the seasonal cycle of EASM as that in the CMAP data (Fig. 3a), with the features that the main rainbelt persists in South China

CPD
8, 3251–3276, 2012

before mid-May, which is also known as the East Asian Spring Persist Rainfall (Wu et al., 2007), and then it moves to the lower-middle reaches of the Yangzi River in June and forms the Meiyu front zone. In July and August, the monsoon precipitation expand further north to North China and gradually retreats towards equator afterward (Fig. 3b). The bias of relatively weaker monsoonal rainfall exists in the tropical regions as shown in Fig. 1b.

3.2 Changes for MH

Due to the change of Earth's orbital parameters in mid-Holocene, the Northern Hemisphere receives more incoming solar radiation during boreal summer that leads to a significant warming over the Eurasia continent beyond 30° N, while the change of TAS is small in low latitude and over the ocean (Fig. 4a). The change of TAS in the northern China is within the range of 1–4 °C as suggested by previous studies of proxy data (Shi et al., 1993). Thus, the land-sea thermal contrast is increased in 6 ka that favors the enhancement of the East Asian monsoon system as shown by the change of the monsoonal circulation. The southwesterly strengthens from the Bay of Bengal to eastern China, while the enhanced upward motion at 500 hpa prevails most regions of East Asia, particularly to the south of Plateau Tibetan and in north China (Fig. 4b).

The change of precipitation follows that of the vertical velocity at 500 hpa as shown in Fig. 4c; the water vapor transport is enhanced by the stronger southwesterly winds that leads to more summer rainfall to the south of Plateau Tibetan and over eastern China. The summer precipitation increases by 5.76 % over the eastern China (100° E to 120° E, 20° N–50° N) at MH, which is similar to the result of PMIP2 model. The precipitation decreases in the tropics, which are related with the anomalous anticyclone over the western Pacific and cooler SST at mid-Holocene.

The seasonal cycle of EASM is also being modified in response to the change of incoming solar radiation in 6 ka that the precipitation decreases before mid-May during the phase of East Asian Spring Persist Rainfall and then it strengthens when the monsoonal rainbelt jumps to the lower-middle reaches of Yangzi River and North China

CPD
8, 3251–3276, 2012

(Fig. 4d). Meanwhile, the retreat of EASM is also delayed by about one month because the enhancement of precipitation persists till the end of September.

3.3 Model spread

Although the PMIP3 model median captures the large-scale characteristics of the EASM, the inter-model differences are large and the regional features differs from one model to the others. As shown in Fig. 1b, the model spread is large for the precipitation in the tropics and to the south of Tibetan Plateau where the model median of summer monsoon precipitation shows a larger deviation from the observation (Fig. 1b). The differences are associated with the different convective schemes in each model. During the MH, the model dispersion for precipitation enlarges mainly in the regions with more monsoonal precipitation while it become smaller in the region with decreasing rainfall, e.g. to the south of Tibetan Plateau and the eastern China and in the tropics. Such changes reflect different model sensitivities in response to the change of insolation.

To better show the model spread, we plot in Fig. 5 the change of TAS in northern Hemisphere and the eastern China (100° E to 120° E, 20° N–50° N) together with the detailed changes of precipitation in three regions (Southern China: 20° N–27° N; Northern China: 35° N–45° N; Yangzi River reaches: 27° N–35° N) of the eastern China for each PMIP3 model. Overall, by excluding some model outliers, the PMIP3 models are relatively closer from one to the other in the change of TAS when compared with the PMIP2 models for both the boreal summer and winter (Fig. 5a). The change of TAS in the eastern China follows that in the Northern Hemisphere, increasing in boreal summer and decreasing in winter, which is dominated by the change of insolation at MH. Almost all the models underestimate the change of TAS in JJA as compared with the range of 1–4 °C in the proxy data (Fig. 5a). It was suggested by some proxy data that the TAS was warmer than present in the eastern China during boreal winter at MH, but no PMIP3 model support such changes that is because the cooling of TAS in the models are dominated by the decreased insolation in winter. The lack of dynamic vegetation in most models may contribute to this model discrepancy so those

CPD
8, 3251–3276, 2012

sensitivity experiments with vegetation forcing are necessary for the understanding of mechanisms.

PMIP3 models show an increased spread of the summer precipitation in the eastern China when compared with that from the PMIP2 models (Fig. 5b). The regional precipitation is featured by an enlarged spread in the southern China and the Yangzi River reaches. Six models simulate consistent increase of precipitation from the south to north in eastern China but with different location of the precipitation maximum, e.g. the CCSM4 shows a large increase of precipitation in southern China but no significant change in northern China and the Yangzi River reaches. Other four models simulate relatively complex patterns of the precipitation change (Fig. 5b). The BCC-CSM simulates a three cores pattern where the precipitation reverses signs between the Yangzi River reaches and the northern and southern China, while the FGOALS-g2 and FIO-ESM show an increased rainfall in northern China but less in the south that are related with the changes in monsoon circulation. The change of precipitation in FGOALS-s2 reduces slightly in both the northern and southern China and remains almost unchanged along the Yangzi River.

4 Discussion

Generally, the magnitude of monsoonal precipitation depends on the large-scale circulation and the atmospheric water vapor content (PRW). For the mid-Holocene, both stronger monsoonal circulation and increased water vapor content would favor the increasing of the summer monsoon precipitation. As shown by the PMIP3 model median, the changes of precipitation are closely associated with the change of vertical velocity at 500 hpa (Fig. 4b and c). Therefore, we plotted in Fig. 6 the change of vertical velocity at 500 hpa (ω 500), which reflects the changes in the large-scale circulations. It shows clearly that the change of monsoon precipitation is dominated by the change of ω 500. Five models (CCSM4, CNRM-CM5, CSIRO-Mk3-6-0, MPI-ESM-P and MRI-CGCM3) show a strengthening of the ω 500 over the most part of eastern China while

CPD
8, 3251–3276, 2012

the weakening of ascend only cover a small portion in this area (Fig. 6), this explains why they simulate stronger monsoonal rainfall in all three regions of the eastern China (Fig. 5b). Regional features can also be identified from the changes of ω 500, e.g. the CSIRO show a maximal change of ω 500 over the lower reaches of Yangzi River (Fig. 6, CSIRO) that favor a larger change of precipitation in this region when compared with the northern and southern China (Fig. 5b). The relationship of the changes between the precipitation and ω 500 is also applied to the other four models of which show a more complex pattern of precipitation change. The change of ω 500 in BCC-CSM shows similar three cores pattern that corresponds the increased rainfall in northern and southern China and less precipitation along the Yangzi River reaches. The ω 500 strengthens in the northern China but weakens to the south in the models of FGOALS-g2 and FIO-ESM that explains the precipitation increases only in the northern China at MH. The change of ω 500 is small in the eastern China so that the change of precipitation is not significant.

Figure 7 shows that the change of water vapor content at MH also favors the enhancement of EASM precipitation in all the model. The PRW increases in the northern part of East Asia, particularly in the northern China, and decreases to the south and over the north-west Pacific (Fig. 7), which is in consistent with the change of monsoonal circulation with stronger southwesterly winds (Fig. 4b). The change of EASM precipitation in the eastern China can be qualitatively derived from the configuration of the changes of ω 500 and PRW, for example in the FGOALS-g2, the ω 500 weakens over the southern China and Yangzi River reaches and strengthens over the northern China, while the PRW increases in northern China and decreases to the south, such configuration explains the changes of monsoon precipitation of FGOALS-g2 as shown in Fig. 5b. This mechanism applies for most of the PMIP3 models, however, the relative importance of the ω 500 and PRW are model dependent that needs further quantitatively analysis.

The climate condition of the Tibetan Plateau (TP) is one of the important factors that influence the activity of EASM (Ding and Chan, 2005). Wu et al. (2007) suggest

CPD
8, 3251–3276, 2012

that during the summer time, the meridional winds and vertical motions forced by the Eurasian continental-scale heating and the TP local heating are in phase over the eastern and central parts of the continent, therefore the monsoon in East Asia intensified. Numerical experiments with atmospheric GCMs (AGCMs) also show that atmospheric heating induced by the rising TP temperatures can enhance East Asian subtropical frontal rainfall (Wang et al., 2008). This mechanism may be applied to explain the large model spread of the precipitation in Yangzi River reaches. Therefore, we plot in Fig. 8 the changes of monsoonal precipitation over the lower reaches of Yangzi River as a function of the changes of TP temperature. The change of simulated TAS over TP show a large spread ranging from −0.7 to +0.3 °C, which may be related with the different simulations of the snow cover in TP. Six models show a positive relationship for the change between the precipitation and TP temperature but the sensitivity is model dependent (Fig. 8). The changes of precipitation in the three models of IPSL-CM5A-LR, MPI-ESM-P and MRI-CGCM3 are more sensitive to the changes of large-scale circulation and water vapor content so that the mechanism from the AGCMs does not applied in these simulations. Since the mechanism of the linkage is found to be through two distinct Rossby wave trains and the isentropic uplift to the east of the TP, which deform the western Pacific Subtropical High and enhance moisture convergence toward the EA subtropical front (Wang et al., 2008), the model's abilities in realistically representing the huge steep topography may have great impact on the coupling between the changes in TP and the EASM activities.

5 Conclusions

Ten coupled models that participated in the PMIP3 are used to investigate their ability in simulating the East Asian Summer Monsoon in the PI simulations and the changes of monsoon circulation and precipitation at mid-Holocene. The model medians are extracted for several variables rather than the model ensemble mean for the analyses. Though with biases when compared to the observations, the PMIP3 model median

CPD
8, 3251–3276, 2012

captures the basic features of the climatology in East Asia, such as the land-sea thermal contrast and the gradually decrease of precipitation towards the inland of the Asian Continent (Fig. 1). The atmospheric circulation of the EASM simulated by PMIP3 model median broadly resembles the pattern as that in the NCEP reanalysis (Fig. 2). However, the vertical velocity at 500 hpa is underestimated by the model median that explains the weaker than observed precipitation at Bay of Bengal, the eastern China and the West Pacific. Two distinct features of EASM, the Meiyu Front and the stepwise medridional displacement of the monsoon rainbelt (Fig. 3) are well represented by the PMIP3 model median.

At mid-Holocene, the PMIP3 model median shows a warming of TAS over the East Asia continent and cooling on the ocean (Fig. 4a), which results from the responses to the insolation change and the different thermal capacity between land and the ocean. The land-sea contrast is enhanced that favors the strengthening of the monsoonal circulation (Fig. 4b). Stronger southwesterly winds and upward motion at 500 hpa prevail over the eastern China that leads to the increase of monsoonal precipitation (Fig. 4c). The seasonal cycle of the EASM is modified by the change of insolation, in which the precipitation weakens in spring and strengthens during the summertime. The monsoon retreat is also delayed by one month at MH (Fig. 4d).

Both in the simulations of PI and MH, the model spread is large in simulating the precipitation of EASM; in particular the model spread enlarges during MH. Analyses that the model spread of summer TAS as simulated by PMIP3 models are relatively smaller when compared with that of the PMIP2 simulations for both the Northern Hemisphere and the eastern China. However, the model spread is larger in simulating the precipitations over the eastern China, particularly in the Yangzi River reaches (Fig. 5b). The changes of monsoon precipitation at MH are associated with the changes in monsoon circulation and the water vapor content. Results show that both the changes in large-scale monsoonal circulation and the water vapor content contribute to the increase of EASM precipitation over eastern China (Figs. 6 and 7). Regional features result from the model's different behaviors of simulating the configuration of changes in monsoon

CPD
8, 3251–3276, 2012

circulation and water vapor content. The positive relationship between the TAS and the subtropical front precipitation that derived from the AGCMs simulations can partially explain the differences among models but it does not apply for all the PMIP3 simulations (Fig. 8). In some models, the precipitation is dominated by the changes of large-scale circulation.

The model spread of precipitation can be resulted from both the model bias in the PI simulation and the different sensitivity to the forcings at MH. The roles of the sea surface temperature (SST) in the Indian Ocean and the Pacific are not yet discussed, for example the cooler than observed SST in the Indian Ocean and the South China Sea may influence the onset and strength of the EASM, the SST bias in the northwestern Pacific may have impact on the Philippine anticyclone that is important to the EASM. The biases may be amplified at a different climate background, therefore, a further study of model's biases are needed.

Acknowledgements. We acknowledge the World Climate Research Programme's Working Group on Coupled Modelling, which is responsible for CMIP, and we thank the climate modeling groups (listed in Table 1 of this paper) for producing and making available their model output. For CMIP the US Department of Energy's Program for Climate Model Diagnosis and Intercomparison provides coordinating support and led development of software infrastructure in partnership with the Global Organization for Earth System Science Portals. The PMIP3 Data archive is supported by CEA and CNRS. More information is available at http://pmip3.lsce.ipsl.fr. This study is jointly supported by the Chinese National Basic Research Program (Grant No. 2010CB950502), the "Strategic Priority Research Program Climate Change: Carbon Budget and Relevant Issues" of the Chinese Academy of Sciences (Grant No. XDA05110301), the National Natural Science Foundation (Grant Nos. 41006008 and 41023002) and the National Key Technologies R&D Program project (Grant No. 2010AA012302).

CPD
8, 3251–3276, 2012

References

Bao, Q., Lin, P., Zhou, T., Liu, Y., Yu, Y., Wu, G., He, B., Li, L., Li, J., Li, Y., Liu, H., Qiao, F., Song, Z., Wang, B., Wang, J., Wang, P., Wang, X., Wang, Z., Wu, B., Wu, T., Xu, Y., Yu, H., Zhao, W., Zheng, W., and Zhou, L.: The Flexible Global Ocean-Atmosphere-Land System Model Version: FGOALS-s2, Atmos. Adv. Sci., submitted, 2012a.

Bao, Y., Qiao, F., and Song, Z.: The historical global carbon cycle simulation of FIO-ESM, Geophys. Res. Abstr., EGU2012-6834, EGU General Assembly 2012, Vienna, Austria, 2012b.

Bartlein, P. J., Harrision, S. P., Brewer, S., Connor, S., Davis, B. A. S., Gajewski, K., Guiot, J., Harrison-Prentice, T. I., Henderson, A., Peyron, O., Prentice, I. C., Scholze, M., Seppä, H., Shuman, B., Sugita, S., Thompson, R. S., Viau, A. E., Williams, J., and Wu, H.: Pollen-based continental climate reconstructions at 6 and 21 ka: a global synthesis, Clim. Dynam., 37, 775–802, 2011.

Berger, A.: Long-Term Variations of Daily Insolation and Quaternary Climatic Changes, J. Atmos. Sci., 35, 2362–2367, 1978.

Braconnot, P., Marti, O., Joussaume, S., and Leclainche, Y.: Ocean Feedback in Response to 6 kyr BP Insolation, J. Climate, 13, 1537–1553, 2000.

Braconnot, P., Otto-Bliesner, B., Harrison, S., Joussaume, S., Peterchmitt, J.-Y., Abe-Ouchi, A., Crucifix, M., Driesschaert, E., Fichefet, Th., Hewitt, C. D., Kageyama, M., Kitoh, A., Laîné, A., Loutre, M.-F., Marti, O., Merkel, U., Ramstein, G., Valdes, P., Weber, S. L., Yu, Y., and Zhao, Y.: Results of PMIP2 coupled simulations of the Mid-Holocene and Last Glacial Maximum – Part 1: experiments and large-scale features, Clim. Past, 3, 261–277, doi:10.5194/cp-3-261-2007, 2007a.

Braconnot, P., Otto-Bliesner, B., Harrison, S., Joussaume, S., Peterchmitt, J.-Y., Abe-Ouchi, A., Crucifix, M., Driesschaert, E., Fichefet, Th., Hewitt, C. D., Kageyama, M., Kitoh, A., Loutre, M.-F., Marti, O., Merkel, U., Ramstein, G., Valdes, P., Weber, L., Yu, Y., and Zhao, Y.: Results of PMIP2 coupled simulations of the Mid-Holocene and Last Glacial Maximum – Part 2: feedbacks with emphasis on the location of the ITCZ and mid- and high latitudes heat budget, Clim. Past, 3, 279-296, doi:10.5194/cp-3-279-2007, 2007b.

Collier, M. A., Jeffrey, S. J., Rotstayn, L. D., Wong, K. K., Dravitzki, S. M., Moseneder, C., Hamalainen, C., Syktus, J. I., Suppiah, R., Antony, J., El Zein, A., and Artif, M.: The CSIRO-Mk3.6.0 Atmosphere-Ocean GCM: participation in CMIP5 and data publication, International Congress on Modelling and Simulation – MODSIM 2011, 2011.

CPD
8, 3251–3276, 2012

Ding, Y. H. and Chan, J. C. L.: The East Asian summer monsoon: an overview, Meteorol. Atmos. Phys., 89, 117–142, 2005.

Dufresne, J.-L., Foujols, M.-A., Denvil, S., Caubel, A., Marti, O., Aumont, O., Balkanski, Y., Bekki, S., Bellenger, H., Benshila, R., Bony, S., Bopp, L., Braconnot, P., Brockmann, P., Cadule, P., Cheruy, F., Codron, F., Cozic, A., Cugnet, D., de Noblet, N., Duvel, J.-P., Ethé, C., Fairhead, L., Fichefet, T., Flavoni, S., Friedlingstein, P., Grandpeix, J.-Y., Guez, L., Guilyardi, E., Hauglustaine, D., Hourdin, F., Idelkadi, A., Ghattas, J., Joussaume, S., Kageyama, M., Krinner, G., Labetoulle, S., Lahellec, A., Lefebvre, M.-P., Lefevre, F., Levy, C., Li, Z. X., Lloyd, J., Lott, F., Madec, G., Mancip, M., Marchand, M., Masson, S., Meurdesoif, Y., Mignot, J., Musat, I., Parouty, S., Polcher, J., Rio, C., Schulz, M., Swingedouw, D., Szopa, S., Talandier, C., Terray, P., and Viovy, N.: Climate change projections using the IPSL-CM5 Earth System Model: from CMIP3 to CMIP5, Clim. Dynam., submitted, 2012.

Folland, C. K., Rayner, N. A., Brown, S. J., Smith, T. M., Shen, S. S. P., Parker, D. E., Macadam, I., Jones, P. D., Jones, R. N., Nicholls, N., and Sexton, D. M. H.: Global temperature change and its uncertainties since 1861, Geophys. Res. Lett., 28, 2621–2624, 2001.

Gent, P. R., Danabasoglu, G., Donner, L. J., Holland, M. M., Hunke, E. C., Jayne, S. R., Lawrence, D. M., Neale, R. B., Rasch, P. J., Vertenstein, M., Worley, P. H., Yang, Z.-L., and Zhang, M.: The Community Climate System Model Version 4, J. Climate, 24, 4973–4991, 2011.

Giorgetta, M. A., Jungclaus, J., Reick, C., Stevens, B., Marotzke, J., Claussen, M., Roeckner, E., Mauritsen, T., Crueger, T., Schmidt, H., Manzini, E., Esch, M., Rast, S., Kinne, S., Zhang, K., Kornblueh, L., Haak, H., Segschneider, J., Six, K., Raddatz, T., Gayler, V., Schnur, R., Legutke, S., Widmann, H., and Glushak, K.: Climate variability and climate change in MPI-ESM CMIP5 simulations, 2012.

Jiang, D. B., Wang, H. J., and Lang, X. M.: Evaluation of East Asian climatology as simulated by seven coupled models, Adv. Atmos. Sci., 22, 479–495, 2005.

Joussaume, S., Taylor, K. E., Braconnot, P., Mitchell, J. F. B., Kutzbach, J. E., Harrison, S. P., Prentice, I. C., Broccoli, A. J., Abe Ouchi, A., Bartlein, P. J., Bonfils, C., Dong, B., Guiot, J., Herterich, K., Hewitt, C. D., Jolly, D., Kim, J. W., Kislov, A., Kitoh, A., Loutre, M. F., Masson, V., McAvaney, B., McFarlane, N., de Noblet, N., Peltier, W. R., Peterschmitt, J. Y., Pollard, D., Rind, D., Royer, J. F., Schlesinger, M. E., Syktus, J., Thompson, S., Valdes, P., Vettoretti, G., Webb, R. S., and Wyputta, U.: Monsoon changes for 6000 years ago: Results of 18

CPD
8, 3251–3276, 2012

simulations from the Paleoclimate Modeling Intercomparison Project (PMIP), Geophys. Res. Lett., 26, 859–862, 1999.

Kalnay, E., Kanamitsu, M., Kistler, R., Collins, W., Deaven, D., Gandin, L., Iredell, M., Saha, S., White, G., Woollen, J., Zhu, Y., Leetmaa, A., Reynolds, R., Chelliah, M., Ebisuzaki, W., Higgins, W., Janowiak, J., Mo, K. C., Ropelewski, C., Wang, J., Jenne, R., and Joseph, D.: The NCEP/NCAR 40-year reanalysis project, B. Am. Meteorol. Soc., 77, 437–470, 1996.

Li, L., Lin, P., Yu, Y., Wang, B., Zhou, T., Liu, L., Liu, J., Xu, S., Huang, W., Xia, K., Pu, Y., Dong, L., Shen, S., Hu, N., Liu, M., Sun, W., Shi, X., Zheng, W., Wu, B., Song, M., Liu, H., Zhang, X., Xue, W., Huang, X., Yang, G., Bao, Q., Liu, Y., Wu, G., Song, Z., and Qiao, F.: The Flexible Global Ocean-Atmosphere-Land System Model: Version g2: FGOALS-g2, Atmos. Adv. Sci., submitted, 2012.

Mitchell, T. D. and Jones, P. D.: An improved method of constructing a database of monthly climate observations and associated high-resolution grids, Int. J. Climatol., 25, 693–712, 2005.

Prentice, I. C., Jolly, D., and BIOME 6000 participants: Mid-Holocene and glacial-maximum vegetation geography of the northern continents and Africa, J. Biogeogr., 27, 507–519, 2000.

Shi, Y. F., Kong, Z. Z., Wang, S. M., Tang, L. Y., Wang, F. B., Yao, T. D., Zhao, X. T., Zhang, P. Y., and Shi, S. H.: Mid-Holocene climates and enviroments in China, Global Planet. Change, 7, 219–233, 1993.

Tao, S. Y. and Chen, L. X.: A review of recent research on the East Asian summer monsoon in China, Oxford Univ. Press, 60–92, 1987.

Voldoire, A., Sanchez-Gomez, E., Salas y Mélia, D., Decharme, B., Cassou, C., Sénési, S., Valcke, S., Beau, I., Alias, A., Chevallier, M., Déqué, M., Deshayes, J., Douville, H., Fernandez, E., Madec, G., Maisonnave, E., Moine, M. P., Planton, S., Saint-Martin, D., Szopa, S., Tyteca, S., Alkama, R., Belamari, S., Braun, A., Coquart, L., and Chauvin, F.: The CNRM-CM5.1 global climate model: description and basic evaluation, Clim. Dynam., online first: doi:10.1007/s00382-011-1259-y, 2012.

Wang, B., Bao, Q., Hoskins, B., Wu, G., and Liu, Y.: Tibetan Plateau warming and precipitation changes in East Asia, Geophys. Res. Lett., 35, L14702, doi:10.1029/2008GL034330, 2008.

Wang, T., Wang, H. J., and Jiang, D. B.: Mid-Holocene East Asian summer climate as simulated by the PMIP2 models, Palaeogeogr. Palaeocl., 288, 93–102, 2010.

CPD
8, 3251–3276, 2012

Wu, G., Liu, Y., Zhang, Q., Duan, A., Wang, T., Wan, R., Liu, X., Li, W., Wang, Z., and Liang, X.: The Influence of Mechanical and Thermal Forcing by the Tibetan Plateau on Asian Climate, J. Hydrometeorol., 8, 770–789, 2007.

Wu, T., Li, W., Ji, J., Xin, X., Li, L., Wang, Z., Zhang, Y., Li, J., Zhang, F., Wei, M., Shi, X., Wu, F., Zhang, L., Chu, M., Jie, W., Liu, Y., Wang, F., Liu, X., Li, Q., Dong, M., Liu, Q., and Zhang, J.: Global carbon budget simulated by the Beijing Climate Center Climate System Model for the last century, J. Climate, submitted, 2012.

Xie, P. P. and Arkin, P. A.: Global precipitation: A 17-year monthly analysis based on gauge observations, satellite estimates, and numerical model outputs, B. Am. Meteorol. Soc., 78, 2539–2558, 1997.

Yao, T. D., Xie, Z. C., Wu, X. L., and Thompson, L. G.: Climatic change since little Ice Age recored by Dundle Ice Cap, Science in China Series B, 34, 760–767, 1991.

Yukimoto, S., Adachi, Y., Hosaka, M., Sakami, T., Yoshimura, H., Hirabara, M., Tanaka, T. Y., Shindo, E., Tsujino, H., Deushi, M., Mizuta, R., Yabu, S., Obata, A., Nakano, H., Ose, T., and Kitoh, A.: A new global climate model of Meteorological Research Institute: MRI-CGCM3 – Model description and basic performance, J. Meteorol. Soc. Jpn., Special Issue, 90a, 23–64, 2012.

Zhao, Y., Braconnot, P., Marti, O., Harrison, S. P., Hewitt, C., Kitoh, A., Liu, Z., Mikolajewicz, U., Otto-Bliesner, B., and Weber, S. L.: A multi-model analysis of the role of the ocean on the African and Indian monsoon during the mid-Holocene, Clim.Dynam., 25, 777–800, 2005.

Zhao, Z. C., Ding, Y. H., Li, X. D., and Wang, S. W.: Evaluation of CGCM climate simulation in East Asian region, J. Appl. Meteorol. Sci., 6, 9–18, 1995 (in Chinese).

Zheng, W. and Braconnot, P.: Characterization of model spread in PMIP2 mid-Holocene simulations of the African Monsoon, J. Climate, submitted, 2012.

CPD
8, 3251–3276, 2012

Table 1. List of PMIP3 coupled models, resolutions and references.

Models	Resolution		References
	Atmos.	Ocean	
BCC-CSM-1	T42L26	360 × 232 L40	Wu et al. (2012)
CCSM4	0.9° × 1.25° L26	320 × 384 L60	Gent et al. (2011)
CNRM-CM5	T127L31	362 × 292 L42	Voldoire et al. (2012)
CSIRO-Mk3-6-0	T63L18	192 × 192 L31	Collier et al. (2011)
FGOALS_g2	2.81° × 2.81° L26	360 × 196 L30	Li et al. (2012)
FGOALS_s2	T42L26	360 × 196 L30	Bao et al. (2012a)
FIO-ESM	T42L26	384 × 320 L40	Bao et al. (2012b)
IPSL-CM5A-LR	1.875° × 3.75° L39	182 × 149 L31	Dufresne et al. (2012)
MPI-ESM-P	T63L47	256 × 220 L40	Giorgetta et al. (2012)
MRI-CGCM3	TL159L48	364 × 368 L51	Yukimoto et al. (2012)

CPD
8, 3251–3276, 2012

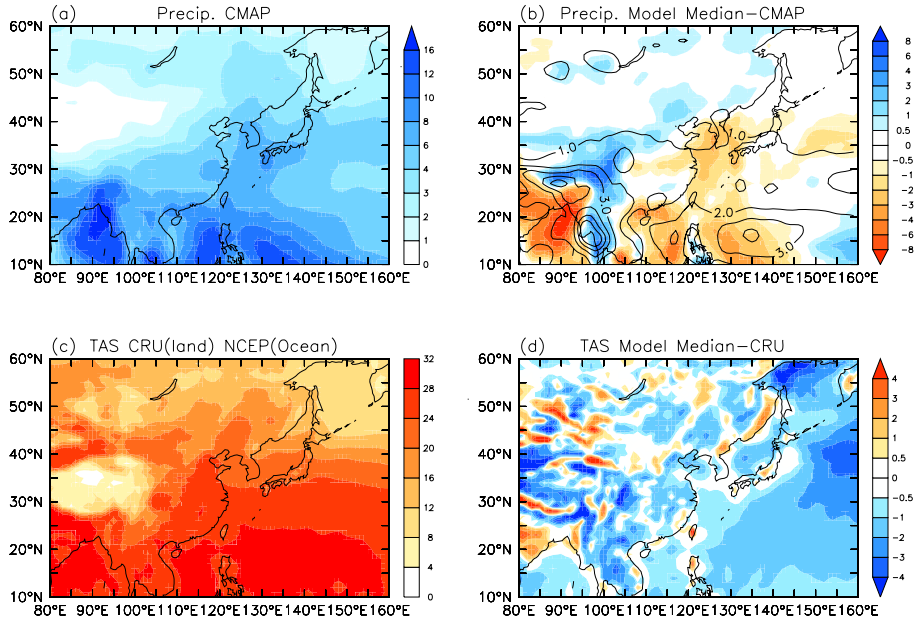

Fig. 1. The observed summer precipitation (JJA, mm d^{-1}) and surface air temperature (TAS, °C) and the differences between PMIP3 model median and the observation. **(a)** summer precipitation of CMAP; **(b)** difference of precipitation between the PMIP3 model median in PI simulation and observation; **(c)** TAS of CRU data; **(d)** difference of TAS between model median 0ka and observation. The contours in **(b)** denote the standard deviation of the ten PMIP3 models for precipitation.

CPD
8, 3251–3276, 2012

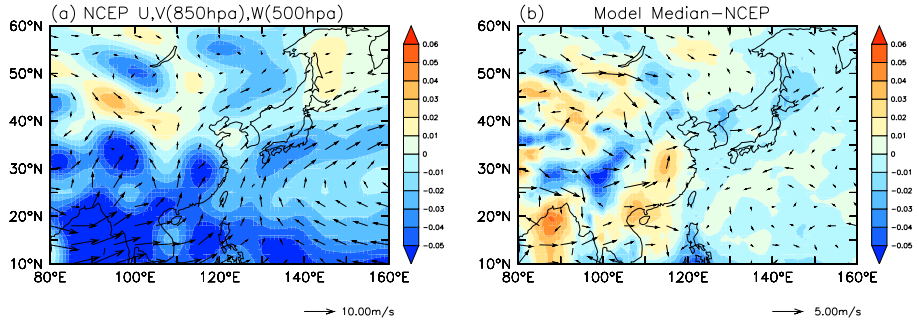

Fig. 2. Monsoon circulation for **(a)** NCEP; **(b)** difference between PMIP3 model median at 0ka and NCEP reanalysis. Vectors are for the wind filed at 850 hpa ($m\,s^{-1}$) and the vertical velocity at 500 hpa (dp/dt) are shown as shaded.

CPD
8, 3251–3276, 2012

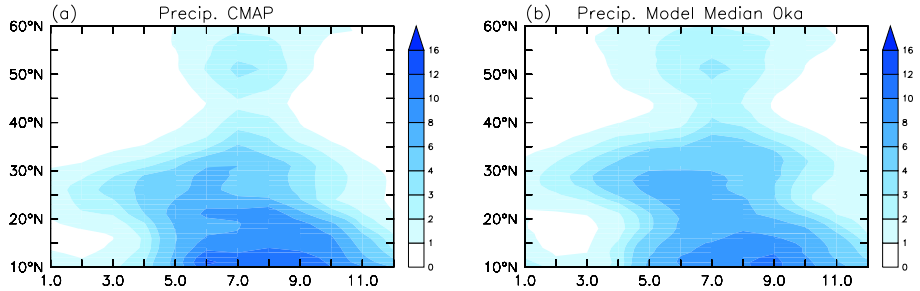

Fig. 3. Seasonal cycle of the EASM, averaged betwwen 100° E and 120° E, for **(a)** CMAP; **(b)** PMIP3 model median for 0ka.

CPD
8, 3251–3276, 2012

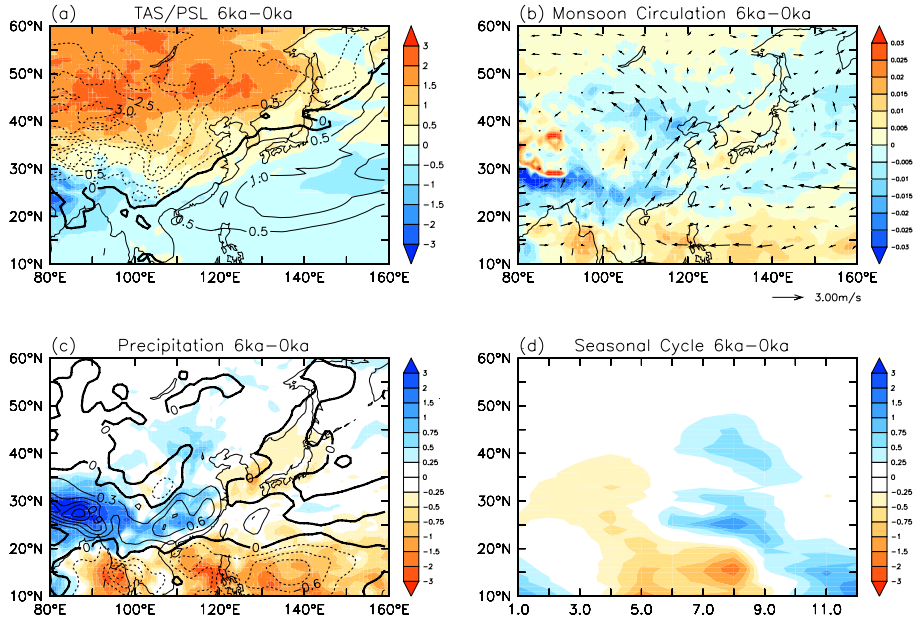

Fig. 4. Changes of PMIP3 model median in 6 ka for **(a)** TAS (shaded, ˚C) and sea level pressure (contour, hpa); **(b)** the monsoonal circulation of the wind at 850 hpa (vectors, $m\,s^{-1}$) and the vertical velocity at 500 hpa (shaded, dp/dt); **(c)** precipitation (shaded, $mm\,d^{-1}$) and the model spread (contour) and **(d)** the seasonal cycle of EASM precipitation ($mm\,d^{-1}$).

CPD
8, 3251–3276, 2012

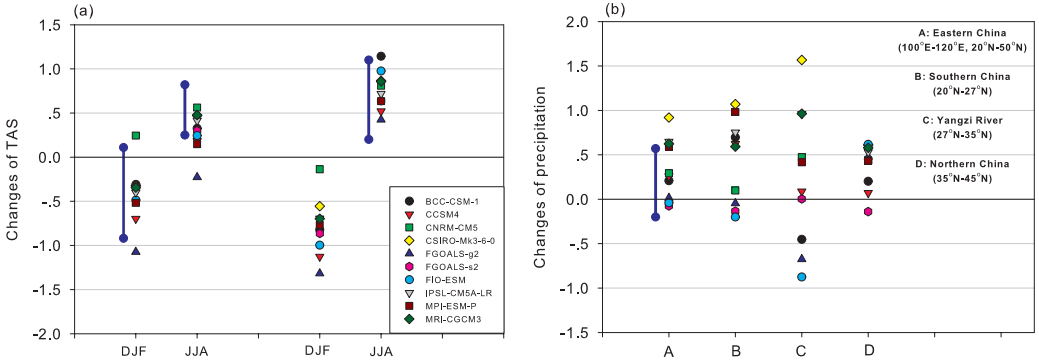

Fig. 5. (a) changes of surface air temperature (TAS, ˚C) in NH and eastern part of China in 6 ka for boreal winter (DJF) and summer (JJA); **(b)**, Changes of the monsoon precipitation in eastern part of China and its three sub domains. Blue lines beside the model symbols indicates the range estimated by the PMIP2 model for the Northern Hemisphere and eastern China from Braconnot et al. (2007a) and Wang et al. (2010), respectively.

CPD
8, 3251–3276, 2012

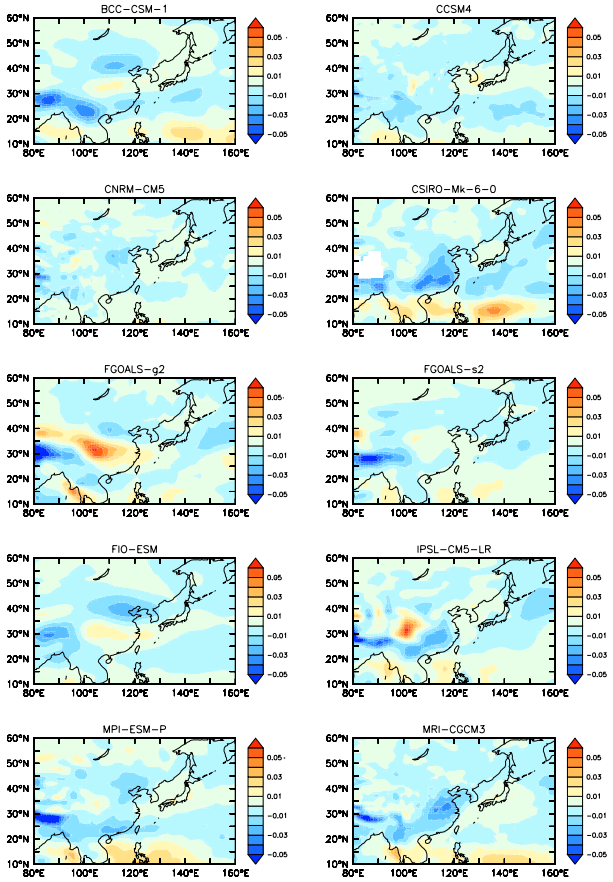

Fig. 6. The changes of the vertical velocity at mid-Holocene for the PMIP3 model in this study. Units: dp/dt.

CPD
8, 3251–3276, 2012

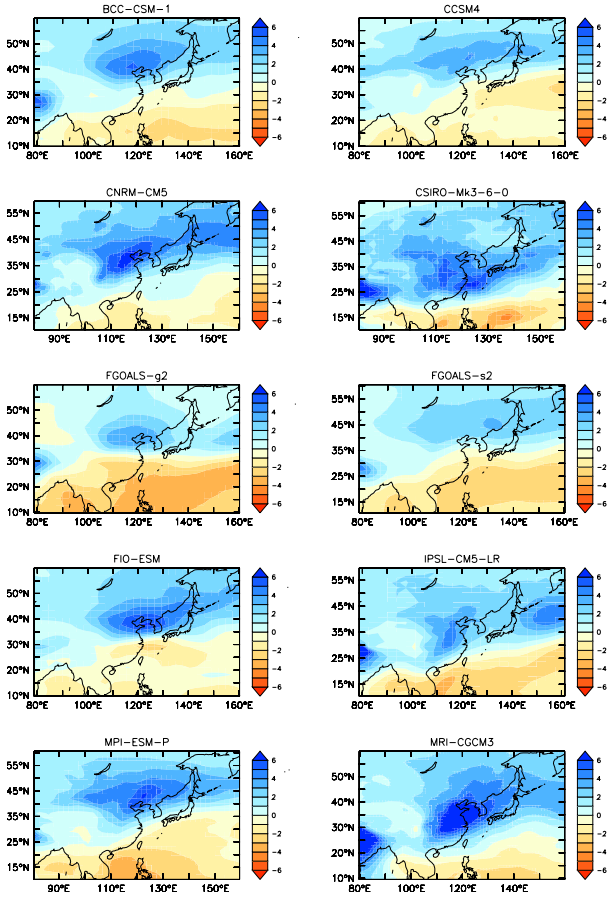

Fig. 7. Same as Fig. 6 but for the changes of water vapor content. Units: kg m^{-2}.

CPD
8, 3251–3276, 2012

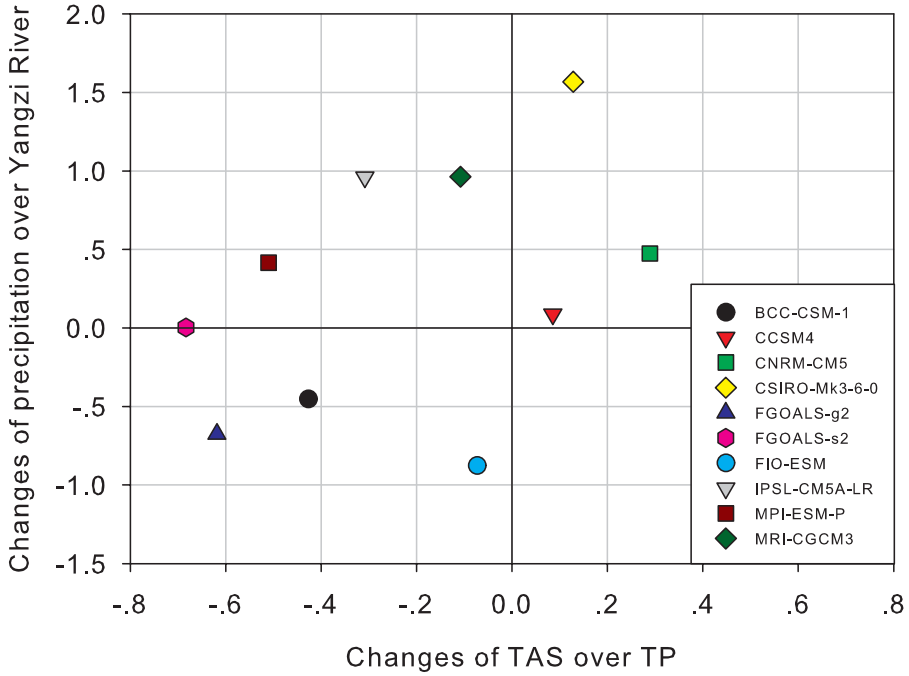

Fig. 8. The changes of precipitation in the lower reaches of Yangzi River (y-axis, mm d^{-1}) as a function of the changes of TAS (x-axis, ˚C) over the Tibetan Plateau (TP, 85˚ E–95˚ E, 25˚ N–35˚ N) during boreal summer.

CPD
8, 3251–3276, 2012